MULTI-LEVEL ANALYSIS OF LOW-COST Z-PINNED COMPOSITE JUNCTIONS. PART 1: SINGLE Z-PIN BEHAVIOR

Javier Toral-Vasquez, Bruno Castanié, Jean-Jacques Barrau, Nicolas Swiergiel

MULTI-LEVEL ANALYSIS OF LOW-COST Z-PINNED COMPOSITE JOINTS

PART 1: SINGLE Z-PIN BEHAVIOR

Javier TORAL VAZQUEZ[1], Bruno CASTANIÉ[1,2], Jean-Jacques BARRAU[1], Nicolas SWIERGIEL[3]

[1] Université de Toulouse, INSA, UPS, Mines d'Albi, ISAE; ICA (Institut Clément Ader)
[2] INSA, 135 Avenue de Rangueil, 31077 Toulouse, France.
[3] EADS IW, 8 rue Marius Terce, 31300 Toulouse, France

ABSTRACT

In the framework of the EU program ALCAS (advanced low-cost aircraft structure), a new Z-Pinning technique was developed by EADS Innovation Works. It was used to manufacture low-cost Z-pinned junction demonstrators (L and T shaped specimens) typical of aeronautical structures. In order to understand load transfer mechanisms in this kind of assembly, a multi-level analysis was performed. Firstly, tension and shear pin behaviour was investigated as well as pin pull-out from net resin. It was demonstrated that the mechanical transfer is mainly through bonding, even when the pins are twisted. Secondly, an analytical model was proposed which predicts the maximum load capacity of a single pin. Finally this study provides the basis for a design methodology to compute ultimate loads of Z-pinned junctions under complex loading.

KEYWORDS.

A 3-Dimensional reinforcement B Stress Transfer C Joints/joining

1- Introduction

As reported by Mouritz [1], z-pinning is one of the most promising reinforcement techniques for classical laminates. Z-fiber®, developed since the eighties by Aztec Inc is the most widespread pinning technique. The technology uses an ultrasonic horn to push pins, held in low density foam, through the laminate before curing. The manufacturing method is detailed in [2]. Although titanium rods were used at the beginning of the technique's development, currently, carbon pins are the most common. For this technology, the pins are typically less than 0.5 mm in diameter and a low percentage value of z-pin density is required to obtain significant reinforcement in the out-of-plane direction. Logically, investigations carried out on z-pinned laminates have focused on the in-plane mechanical properties, their delamination behavior and the impact or post-impact response [3]. Z-pinning slightly decreases the in-plane mechanical properties of laminates due to the pin insertion process [4-7] which creates an undulation of the fibres (see Figure 1). The eye-shaped resin pockets produced can influence the response under thermal loading or fatigue [8-10]. As expected, the delamination strength can increase significantly in mode I [11-13]. The mechanisms that increase the delamination strength are the bridging forces that are created while the pins are pulled out from the laminate under opening loads. The strength of an interface can also be reinforced under shear loading by Z-pinning [12]. In this case the behaviour of a pin is complex. It is subjected to a combination of pull-out, internal shear which can cause splitting of the pin and transverse shearing. Moreover, the failure mode is also dependent on the stiffness of the resin area and the laminate itself [12]. Pin behaviour under pull-out loadings has been investigated experimentally [13], [14] and numerically [15] showing a two or three slope load-displacement response. Dai et al have also shown that small diameter pins are more efficient than larger ones. The research carried out on the Z-Pinned joint will be

presented in part 2 of this publication. It will be demonstrated that the behavior of the junction under pull-out, shear and unfolding is globally homothetic to the mechanical behaviour of a pin. In spite of the works on the Z-pinned structures, the applicability of the results on EADS IW technology is still to be demonstrated. Moreover, no sizing methodology was undertaken to design joints. So, in the following section, the new pinning technique will be presented and the choice of a multi-level analysis justified.

2- EADS Innovation technology and methodology of analysis.

In the framework of the European ALCAS program (Advanced Low-Cost Aircraft Structure), investigations were conducted to develop low-cost composite junctions enabling automatic manufacturing and diminishing or avoiding manual lay-up. A new technology of automatic insertion of Z-Pins developed by EADS IW is analysed in this study [16]. The technology uses twisted carbon fibre pins produced by Hexcel. Their diameter here was 0.7mm and their length 40 mm (Figure 2). The pin insertion system is held in a 7-axis machine so the pinning process can be automated (Figure 3). The pins are longer than Z-fiber® carbon pins [2] in order to be able to manufacture T-joints without a stiffener flange, thus creating a “low-cost” junction. A vibrating holed needle with the Z-Pin inside (see Figure 3) penetrates into a dry preform provided by Dassault Aviation. Once the desired depth is reached, the needle comes out leaving the Z-Pin inside the preform (Figure 4). Finally, the pins are cut before injection of the preform using an resin transfer molding (RTM) system. The objective of the present study was to provide users a pre-sizing method for this new technology. In aeronautics, such sizing methods are related to two concepts: the notion of limit and ultimate loads and the “no-crack growth” principle. The limit loads are the maximum loads that any aircraft can be subjected to during its life. Under the

limit loads (LL), the structure must be calculated for use under fatigue loading and it is the reason why absence of crack growth is mandatory for composite parts. The ultimate loads (UL) are equal to 1.5 LL and the structure must sustain this load only statically. This ability is validated by static certification tests which are required to allow the aircraft to fly. Between the Limit and the Ultimate Loads cracks can propagate because a real aircraft will never see such loadings during its life. According to the literature, delamination energy is absorbed by Z-pins via frictional pull-out so this technology does not provide real advantages until limit loads. Moreover, we show in the companion paper that cracks initiate in joints at about the same loads with and without Z-pinning as already pointed out by Greenhalgh et al [17]. However, real structural gains are demonstrated for ultimate loads because, for a classical bonded joint, the propagation of a crack is faster. So the design methodology for such pinned joints can be separated into two: classical design methods for limit loads which are not the subject of the present research and a new pre-sizing method for ultimate loads. The assumptions made and the methodologies adopted in this paper are presented hereafter.

As for Z-fiber technology, the insertion process creates resin pockets around the pin as shown in Figure 1. In the present case, visual observations indicate that the pins are surrounded mostly by resin. Only few laminate fibres are in contact with the pin, probably due to the fact that the diameter of the needle is necessarily greater than the diameter of the pin. Thus, the main assumptions made during this investigation were:

- Load transfer between pin and surrounding matrix is mainly due to bonding.

- The behaviour of a pinned joint is homothetic to the behaviour of a single Z-pin.

The observations made led us to present a multi-level analysis of pinned joints (Figure 5). The first level includes pin and resin elementary mechanical characterisation. Resin analysis consisted of a standard matrix characterisation showing slight non-linear behaviour [18] and will not be presented here. Only single pin tests under traction and shear will be presented. The second level considered pin pull-out behaviour when bonded in resin with an analytical model to predict pull-out strength. At this level, pull-out behaviour of single pins inserted into laminates will show similarities with pull-out behaviour from resin thus validating the first assumption. A numerical model is developed able to calculate the debonding load. The third level will be presented in the companion paper and will deal with L and T shaped pinned structural joints tested under tension, shear and unfolding loads. The test results demonstrated the utility of pinning structural joints from a static point of view. Ultimate loads were calculated assuming homothetic behaviour of the pins in the structure and no interaction between pins. The pins were modelled as non-linear springs. The non-linear laws under tension and shear of the springs were obtained from the combined experimental and numerical results of the first and second levels of the analysis thus demonstrating the suitability of the pre-sizing method presented.

3- Single pin testing

3.1 Tension

The carbon pins used in this study consisted of T700 carbon fibre tows impregnated with M18 epoxy matrix (Figure 2 (a)). The carbon fibre tows were slightly twisted to obtain an irregular outer surface (Figure 2 (b)). The pins were delivered with a matrix polymerisation of 80%, to be completed during joint manufacturing to

allow chemical links with laminate resin to be created. Carbon pins were tested under tension to measure their strength and stiffness. Before testing, the pins were cured for 3 hours at 180ºC to complete resin polymerisation. The tests were performed on an Instron 10kN tension test machine. The tension load was applied on a single pin through mechanical grips. To protect the pin from damage by the grips, small carbon-epoxy plates were bonded to both pin ends. The plates were 2 mm thick and had a hand-made V-shaped groove to fit the pin ends (see Figure 6). The two plates were not in contact to allow good clamping of the pin. Load was measured by the load cell while two inductive sensors gave the displacements [18].

Three tests were performed. Load/displacement curves are shown in Figure 7. The curves show a slight non-linear behaviour with a decrease of the tangent modulus for the highest load values. The same non-linear behaviour has been observed for steel cables also composed of twisted tows [19]. Thus, it seems very likely that the source of the pins' non-linearity is the twist in the carbon tows. From the test results, a stress/strain behaviour law was established using engineering stress and strains (based on initial circular section). The behaviour of the 0.7 mm diameter pins is shown in Figure 7. It can be fitted with a polynomial law of degree 3 using least squares [18] so that a tangent Young's modulus at low strains of 92 092 MPa can be obtained as well as a final tangent Young's modulus of 32 255 MPa before failure. The pins failed most often near the end grips. The order of magnitude of the mean maximum stress was 2000 MPa, indicating that the test method used is globally correct as this value matches well classical UD carbon-epoxy tensile strengths.

3.2 Shear

Pins were tested under shear loadings using a specially designed test assembly. The test assembly consisted of two coaxial cylinders with a hole perpendicular to the cylinder axis as shown in Figure 8. The external cylinder was attached to a rigid rig fixed to the machine frame. The internal cylinder slipped inside the external one to apply a shear loading on the pin in the hole. Three pins were sheared with just one end in the device and three others with the pin crossing through the two holes. The cylinders were made of brass to minimise friction and for manufacturing reasons. The load-displacement curve of the pin shear test is presented Figure 9. The first stage, where load increases slightly corresponds to the displacement due to the clearance and to initial contact of the twisted pin in the test device. This initial contact also involves crushing the rough points on the pins. This is followed by a linear load increase until fragile pin failure. The strength of the pins and the shear stiffness are reported in Table 1. The stiffness value is probably influenced by the clearance between the test rig components (measured at 0.1 mm), a point which will be discussed in the second paper which focuses on pinned joint modelling and testing. From these values of strength and stiffness, pin shear behaviour can be modelled as a linear fragile behaviour law.

4- Pull-out testing

Pull-out tests were performed on pins bonded in epoxy resin. Specimens consisted of a carbon pin bonded in the centre of a resin block with (Figure 10(a)). The specimens were manufactured using a metal mould of internal dimensions 50 x 50 x 15 mm (see Figure 10(b)). The specimen preparation process in fully described in [18]. The first step involved heating the resin to 120°C for 10 min in order to reduce its viscosity. Then, the still liquid resin was poured into the mould while pin was held

vertically. When filling the mould, resin height was obtained with a precision of +/- 1 mm. The specimen was then cured following the appropriate curing cycle. Different pin-resin bonded lengths were tested by modifying resin block height. Twenty-three specimens were manufactured. To carry out the pull-out tests, the vertical displacement of the specimen was blocked over the upper surface of the resin brick 5 mm from the pin centre as seen in Figure 11 (a). Pin pull-out tests were performed using a standard tensile machine and a special grip to hold the upper part of the pin to apply the load (see Figure 11 (b)). The applied load and the vertical displacement of the pin were recorded during the test by two Linear Variable Differential Transformer (LVDT) sensors. A mass was added to minimize dynamic effects during fragile failure. A zoom on the grids is shown in figure 11 (c). Initial tests were conducted with dial recorders to validate the measures given by the LVDT.

Figure 12 shows three typical load-displacement curves from pull-out tests. Three stages can be distinguished: first, the pin's elastic deformation before reaching maximal load. This is followed by an applied-load drop due to resin-pin interface failure and, finally, the debonding stage where friction effort decreases while the pin slips inside the resin block. For all the tests, the initial debonding load spike was higher than the friction load during the third stage. These three stages have been described and observed during pin pull-out tests from laminates performed by Dai et al [13]. Finding the same global behaviour gives the first similarity indication between pins bonded in pure resin and pins inside laminate. We investigated the influence of bond length over maximum pull-out load. Twenty-three pull-out tests were performed with different bonded-lengths: from 2 to 12 mm. The results are presented in terms of maximum pull-out load versus bond length. Figure 13 shows the test points. The test results are quite scattered. Some post-mortem analysis using scanning electron

microscopy (see Figure 14 and 15) showed that the fracture surface matches up with the pin-resin interface but can also go though the pin itself. This observation indicates that the pin to resin joint is as resistant as pin matrix and fibre joint. However, the irregular pin surface (see figure 2) that produces different stress concentration points at the pin-resin interface for each specimen can produce scatter. The scatter could also be due to the influence of the meniscus on the upper face of the resin block. The radius of the meniscus was measured and scatter also appeared with radii of 1.5 mm to 4 mm for a block thickness of about 5 mm and a radius reaching 9 mm for block of 11.6 mm height. As this area is also an area of stress concentration, the differences can also lead to scatter. Finally, even if tests were made on some specimens showing no defects, it is still possible that voids appear in the resin block or at the interface. The points in Figure 13 can be extrapolated to the origin as, for a null bonded length, the resistance is zero. Thus, despite the scatter, a general trend can be observed: pin resistance increases for bond lengths between 0 and 4 mm. For bond lengths over 4 mm, the debonding load remains fairly constant. This behaviour corresponds to that of a typical bonded joint where, after a given bond length, strength saturates.

5- Pull-out modelling

The pin pull-out process presents some similarities with fibre pull-out from resin. Fibre pull-out tests were developed to characterise the fibre/resin interface by measuring the maximum shear stress at the interface. Several models are proposed in the literature to analyse fibre pull-out. Analytical models from Zhang et al [20] and Fu et al [21] provide the stress distribution at the fiber/resin interface for a fibre bonded in net resin and a fibre bonded in net resin and surrounded by orthotropic

material respectively. Based on these two models, a new model was developed to calculate the stress state at the pin/resin interface for the configuration of pin pull-out tests presented above. The model considers the geometry and configuration shown in Figure 16. Full details of the calculation can be found in reference [18].

The pin is bonded in a resin cylinder of radius c. An equilibrium occurs between the pullout force F_0 and the contact pressure at the upper surface of the resin cylinder for radius greater than b. Pin and resin are assumed to be elastic-isotropic materials. For a given horizontal section, the load balance over the X component can be written as follows:

$$\pi a^2 \sigma_x^f(x) + 2\pi \int_{r=a}^{r=b} \sigma_x^{m1}(r,x) r dr + 2\pi \int_{r=b}^{r=c} \sigma_x^{m2}(r,x) r dr = 0 \qquad \text{(Eq 1)}$$

Indices–f, m1 and m2 indicate the pin, the resin for radius bellow b and the resin for radius bigger than b respectively. According to Fu et al [20], shear stress in the resin can be written:

$$\tau_{mi}(r,x) = \frac{p_{mi}(x)}{r} + q_{mi}(x) r \qquad for \qquad i = 1,2 \qquad \text{(Eq 2)}$$

Where p_m and q_m are the functions to be determined. The stress balance between shear stress at the pin/resin interface $\tau_c(x)$ and normal stress inside the pin led to:

$$\frac{d\sigma_x^f(x)}{dx} = \frac{2}{a} \tau_c(x) \qquad \text{(Eq 3)}$$

In the same way, stress balance between shear stress inside the resin at r=b and the axial stress over the outer region of the resin can be written:

$$-2\pi b \tau_{m2}(b,x) + 2\pi \int_{r=b}^{r=c} \frac{d\sigma_x^{m2}(r,x)}{dx} r dr = 0 \quad \text{(Eq 4)}$$

At r=a and r=b, shear stress over the different domains is related by the following expressions:

$$\begin{aligned}&\tau_{m1}(b,x)=\tau_{M}(b,x)=-\tau_{m2}(b,x)\\&\tau_{m1}(a,x)=-\tau_{C}(x)\end{aligned}\qquad\text{(Eq 5)}$$

Considering that normal radial and hoop stress are negligible compared to axial stress, the axial strains can be written as follows:

$$\frac{\boldsymbol{du_x^j(r,x)}}{\boldsymbol{dx}}=\varepsilon_{xx}^{j}(\boldsymbol{r},\boldsymbol{x})=\frac{\sigma_x^j(\boldsymbol{r},\boldsymbol{x})}{\boldsymbol{E_j}}\qquad\textbf{for}\qquad \boldsymbol{j}=\boldsymbol{f},\boldsymbol{m}1,\boldsymbol{m}2\quad\text{(Eq 6)}$$

The boundary conditions are:

$$\begin{aligned}&\tau_{m2}(c,x)=0\\&\sigma_x^f(x=L)=\sigma_0\\&\sigma_x^f(x=0)=0\end{aligned}\qquad\text{(Eq 7)}$$

Solving the above equations [18], gives the axial stress distribution along the pin and also the shear stress distribution along the pin/resin interface:

$$\begin{aligned}\sigma_x^f(x)&=\frac{\sigma_0}{\sinh(\lambda L)}\cdot\sinh(\lambda\cdot x)\\\tau_c(x)&=\frac{a\cdot\lambda}{2}\frac{\sigma_0}{\sinh(\lambda L)}\cdot\cosh(\lambda\cdot x)\end{aligned}\qquad\text{(Eq 8)}$$

Where λ is a function of radii a, b and c and of the mechanical properties of pin and resin. The very complex expression of λ is given in Appendix 1. The shear stress distribution shows its maximum value at the highest point of the interface x=L. Thus, it can be assumed that pin disbonds from resin when the shear stress reaches a critical value at this point. This assumption involves:

$$\tau_{MAX}=\frac{\lambda}{2}\cdot\frac{F_{\max}}{\pi\cdot a\tanh(\lambda\cdot L)}\qquad\text{(Eq 9)}$$

As the maximum shear stress is an interface pin/resin characteristic, the debonding load can be written as follows:

$$F_{\max}(L) = \frac{2 \cdot \pi \cdot a}{\lambda} \tau_{\max} \tanh(\lambda \cdot L) \qquad \text{(Eq 10)}$$

From this expression, the critical shear stress of the pull-out tests can be obtained by fitting the $F_{max}(L)$ analytical expression with the experimental data points. In this manner, a critical value of 58 MPa was found corresponding to the curve in Figure 15. Thus, the analytical model gives a reference for the variation of the pull-out load versus bond length. The scatter of the experimental points makes it difficult to validate this curve but overall, it follows the main trend. However, some discrepancies can be found, in particular for bond lengths above 8 mm where the model seems to under-estimate the pull-out strength experimentally obtained. It is possible that for lengths of over 8 mm, cracks have to propagate in the pins thus increasing the failure energy required (see figure 14 and 15).

The analytical model is based on strong assumptions, especially the isotropic linear behaviour of resin and pin and the fact that the menisci around the pin were not take into consideration. In order to estimate the validity of the analytical model, its results were compared to those provided by a FEM model. The FEM model was developed using SAMCEF software [22] and consists of an axisymetric model including the resin menisci around the pin and with boundary conditions in line with the tests. The geometry, the mesh and the boundaries of the model are reported in Figure 18. The typical size of the elements was 0.01 mm in the most refined area; using smaller elements did not change the stress values obtained.

The mechanical properties of pin and resin were those obtained from the characterisation tests presented in section 3. The pin material traction law in the axial direction corresponds to the curve shown in Figure 7. Pin transversal properties correspond to a typical carbon-epoxy UD ply (E_t=9000 MPa, ν_{lt} = 0.25, G_{lt} = 4000 MPa). Resin is assumed to present an isotropic plastic behaviour as determined through tension tests [18]. The shear modulus of the resin used was 1443 MPa and ν =0.3. The first study compared the shear stress at the pin/resin interface between the FE model and the analytical model. The case study corresponds to a resin block 5.5 mm high and an applied load of 300N. This load level was of the same order of magnitude as the debonding load measured during pull-out tests. The shear stress comparison in Figure 19 shows a good agreement between the two models. The agreement was worse in the upper part of the interface where the analytical model over-estimated shear stress. The mismatch could be explained by the fact that the analytical model did not consider the plastic behaviour of the resin. Thus, the real maximum value of the shear stress should be close to the FEM results and consequently lower than the critical shear stress used by the analytical model. After shear stress comparison, the FE model was employed to calculate the changes in debonding load with the bond length. Two criteria are proposed: the Tresca criterion and a maximum strain based criterion. To compare analytical and numerical models, the critical criteria value was set at a common point over the curve of strength vs. bond length for the two models. This point corresponds to L=5.5 mm and F_{max}= 328 N given by the analytical model after matching the experimental results. At this point, the values are 48 MPa for the Tresca criterion and 0.0409 for the maximum strain criterion. Then, by modifying the bond length, the maximum applied load that fulfils failure criteria was calculated. Figure 17 shows debonding load vs. bonded length for

both criteria applied to the FE model compared to analytical model results. The analytical model and the two criteria used with the FE model present globally the same variation, in particular with a maximum load plateau for bond lengths over 6 or 7 mm. The Tresca criterion gives strength values higher than strain-based criteria for bond lengths bellow 5 mm. This could be attributed to resin plastic behaviour. Indeed, as the stress vs strain relationship is no longer linear, close to the failure point strains increase faster than stress explaining the fact that the Tresca criterion is more conservative. Comparison between the analytical and numerical models shows that, despite the simplifying assumptions made, after a single experimental adjustment, the analytical model seems valid, especially for low bond lengths. This point is quite important in practice as in a typical aeronautical pinned T-joint (see Figure 20), pins always fail in pull-out by debonding from the skin, where the insertion length is shorter. Despite its complexity, the FE model also presents some limitations as it cannot explain the load scatter encountered in the test results.

6- Pull-out from laminates

The objective of this part of the study is to analyse the behaviour of a single Z-pin in a laminate and to compare it with the behaviour in net resin. Specimens with a single pin which mimics the inclusion of pins in the web with different depths were manufactured (see Figure 21). Specimens were made with pins in the skin (replacing the resin block in figure 10 by a laminate) but it turned out to be impossible to manufacture in an autoclave. The specimens consist of two half carbon/epoxy plates jointed by a single pin and separated by foam with two layers of Teflon to avoid bonding between the edges of the plates. The plates were made of twelve 914/G803 pre-preg tissues for a total thickness of 3.4 mm. Pins were 0.7 mm in diameter and 40 mm long. During lay-up, the pin was placed manually in the middle of the layers of

laminate (see Figure 22 (a)) and the insertion depth L in one of the two plates is checked (see Figure 22 (b)). Table 2 lists the 47 specimens tested, obtained from 8 plates and an insertion depth varying from 3 to 20 mm. Pull-out tests were performed by fixing both specimen ends inside the 10kN Instron tension machine grips. The applied load was measured by the machine load cell while displacements were obtained from LVDT sensors. In order to isolate and correct any parasitic rig displacement, some tests were instrumented with cameras to obtain specimen displacement by digital image correlation (see Figure 23).

Load-displacement curves are globally similar to those obtained from pin pull-out from net resin as presented in Figure 12. However, looking at a smaller displacement scale, a load-displacement curve indicating a different behaviour of the type shown in Figure 24 for a 15 mm insertion depth, can be observed. Indeed, the decrease in tangent modulus is significant before reaching the maximum load level. By comparing with the non-linear response of the free length of the Z-pin between the two plates (3mm), it can be shown that other mechanical properties are involved [18]. For a better understanding of the mechanical process behind this phenomenon, tests were stopped at different stages of debonding. Micrographic analysis of specimen 5G, stopped before reaching the maximum load, shows some cracks at the pin/matrix interface (Figure 25 (a)). Crack length is around 7 mm beyond which the interface seems not to be damaged (Figure 25 (b)). In contrast, in specimen 6G, stopped after final load drop-off, shows the pin fully debonded from the resin (Figure 25 (c)). Here, cracks appear all over the interface as well as in areas inside the pin itself (figure 25 (d)). Crack propagation inside the pin may be due to the twisted tows that form the pin interfering with the crack path. Thus, the main difference between pin pull-out from resin and pull-out from laminate is the more progressive debonding of pin from

the laminate. Micrographic analysis showed that the tangent modulus decrease was due to initiation of interface cracking.

The influence of insertion depth on pin pull-out behaviour can be analysed by comparing the plots in Figure 26. The curves appear to be globally superimposed over both the first quasi-linear load increase and the second slope corresponding to interface crack propagation. The maximum applied load increased as the insertion length increased. From these curves, it is possible to obtain the crack initiation load level and the maximum load level for each insertion depth (Figure 27). The next step consists of comparing these results with experimental and numerical values of pin pull-out from net resin. The debonding load of a pin bonded in resin is comparable to the load initiating pin interface cracks in laminates (Figure 28). The crack initiation load increase for insertion depths of over 6 mm is less steep here than for the maximum applied load presented above. Note that the pin requires a higher load to be pulled out from a laminate than from resin if the insertion depth is greater than 6 mm. These analyses are consistent with the failure scenarios identified through micrographic analysis and they indicate that crack initiation at the pin/resin interface or pin/laminate interface occurs for the same load level. If the pin is bonded in net resin, the crack spreads sharply over the whole interface and causes pin debonding while if the pin is inserted in a web, crack propagation at the interface shows a stable stage before complete debonding.

The initial assumption that pin behaviour in a laminate is similar to that in net resin is only partially true. For insertion depths of up to 6 mm, it seems to be a fairly accurate approximation and the analytical model can provide a maximum force. For deeper insertion, however, it is no longer the case but the ultimate load is underestimated which remains acceptable in pre-sizing. Finally, in our specimens we

placed the pins manually between two plies without using the vibrating needle before curing under pressure. Thus, there is certainly less space between the plies and the pins, and more numerous contacts. The contacts may play the role of crack arrestor increasing the energy required for crack propagation and thus the maximum force. They probably provide an upper boundary for this force by comparison to a pin in a skin (see picture 20). At this stage of the study, the assumption of identical behaviour in net resin and in laminate remains viable even if certain limitations and special behaviour in a web were highlighted. In fact, in the companion paper, we report that pins never debond from web but only from skin even with an equal insertion depth, thus the load calculated by the numerical model is able to predict the debonding load. Nevertheless, to achieve an accurate representation of behaviour of a pin inserted into a web, a more complex model able to represent crack propagation between a pin and a laminate should be developed but this point was beyond the scope of a pre-sizing method.

7- Conclusions.

In this first part of the study, the behaviour of single Z-pins was analysed. Tensile and shear strength of the pins was measured and will allow the pinned joints to be modelled, as reported in the second part of this publication. Then, an experimental study of pin pull-out from net resin was carried out. Pin debonding seems to be controlled by shear stress at the pin/resin interface as for generic bonded joints. An analytical model based on the principles of continuum mechanics made it possible to find this behaviour with only one experimental adjustment.

Also pull-out test of a pin inserted into laminate, which mimics the pin in a web was carried out.. The main difference with pin in neat resin is stable crack

propagation at the pin/laminate interface. However, crack initiation load level is mostly the same for both pins in net resin and pins in laminate which is coherent with sudden interface crack propagation when the pins are bonded in net resin. However, the debonding load increases with pin insertion depth. This effect is probably due to the fact that pin is parallel to the ply in this experiment. Stable crack propagation requires more energy and can explain why, in joints, pins always debond from the skin even with equal insertion depth. To design joints for ultimate load, it is necessary to know the maximum force on the pin/laminate junction and the assumption that the debonding load of a Z-pin can be calculated with the numerical model remains valid and will be confirmed in the second part of this article.

8- Acknowledgment

The authors would like to thank Thierry Vilain (Dassault Aviation and ALCAS WP3 leader) and Patrice Lefebure (EADS IW) for their support.

9- Appendix

The expression of coefficient λ is given below. The details of the calculation can be found in [17].

$$\lambda = \frac{-\beta_2 - \sqrt{\beta_2^2 - 4\beta_1\beta_3}}{2\beta_1} \qquad \text{(Eq A-1)}$$

With:

$$\beta_1 = \frac{C_{32}A_{12} - C_2A_{13}}{C_4} \qquad \text{(Eq A-2)}$$

$$\beta_2 = A_{12} + \frac{C_{32}A_{11} - C_1A_{13}}{C_4} \qquad \text{(Eq A-3)}$$

$$\beta_3 = A_{11} \qquad \text{(Eq A-4)}$$

Where:

$$C_1 = \frac{E_m}{E_f}\frac{b^2 - a^2}{2} \quad \text{(Eq A-5)}$$

$$C_2 = \frac{b^2 - a^2}{2} A_{mb1} \quad \text{(Eq A-6)}$$

$$C_3 = \left[\frac{b^2 - a^2}{2} A_{mb2} + \frac{2(1+\nu_m)b}{c^2 - b^2} I_1 \right] \quad \text{(Eq A-7)}$$

$$C_{32} = -\frac{c^2 - b^2}{2b} C_3 \quad \text{(Eq A-8)}$$

$$C_4 = -\frac{c^2 - b^2}{2} \quad \text{(Eq A-9)}$$

With:

$$A_{mb1} = \frac{(1+\nu_m)a^2}{(b^2 - a^2)}\left[\frac{1}{2}(b^2 - a^2) - b^2 \ln\frac{b}{a} \right] \quad \text{(Eq A-10)}$$

$$A_{mb2} = \frac{2(1+\nu_m)b}{(b^2 - a^2)}\left[\frac{1}{2}(b^2 - a^2) - a^2 \ln\frac{b}{a} \right] \quad \text{(Eq A-11)}$$

$$I_1 = c^2\left(\frac{c^2}{2}\ln\frac{c}{b} - \frac{c^2 - b^2}{4} \right) - \frac{(c^2 - b^2)^2}{8} \quad \text{(Eq A-12)}$$

And:

$$A_{11} = a^2 + 2(M_1 + C_1) \quad \text{(Eq A-13)}$$

$$A_{12} = 2(M_2 + C_2) \quad \text{(Eq A-14)}$$

$$A_{13} = 2(M_{32} + C_{32}) \quad \text{(Eq A-15)}$$

With:

$$M_1 = \frac{E_m}{E_f}\frac{(b^2 - a^2)}{2} \quad \text{(Eq A-16)}$$

$$M_2 = \frac{(1+\nu_m)a^2}{(b^2 - a^2)}\left[\frac{(b^2 - a^2)^2}{8} + b^2\left(\frac{b^2 - a^2}{4} - \frac{b^2}{2}\ln\frac{b}{a} \right) \right] \quad \text{(Eq A-17)}$$

$$M_3 = \frac{2(1+\nu_m)b}{(b^2-a^2)}\left[\frac{(b^2-a^2)^2}{8} + a^2\left(\frac{b^2-a^2}{4} - \frac{b^2}{2}\ln\frac{b}{a}\right)\right] \qquad \text{(Eq A-18)}$$

$$M_{32} = -\frac{c^2-b^2}{2b}M_3 \qquad \text{(Eq A-19)}$$

10- References.

[1] Mouritz A.P.: Review of z-pinned composite laminates. Composites Part A 2007; 38(12): 2383-2397.

[2] Partridge I.K., Cartie D.D.R., T. Bonnington.: Manufacture and performance of z-pinned composites. Advanced Polymeric Composites, ed. G. Shonaike and S. Advani, CRC Press, FL, 2003.

[3] X Zhang, L Hounslow, M Grassi. Improvement of low velocity impact and compression-after-impact performance by z-fibre pinning. Compos Sci. & Tech. 66 (2006) 2785-2794.

[4] Chang P., Mouritz A.P., Cox B.N.: Properties and failure mechanisms of z-pinned laminates in monotonic and cyclic tension, Composites Part A 2006; 37(10): 1501-1513.

[5] O'Brien T.K., Krueger R.: Influence of compression and shear on the strength of composite laminates with z-pinned reinforcement. Applied Composite Materials 2006; 13: 173-189

[6] Mouritz A.P.: Compression properties of z-pinned composite laminates. Composites Science and Technology 2007; 67(15-16): 3110-3120.

[7] Steeves C.A., Fleck N.A.: In-plane properties of composite laminates with through-thickness pin reinforcement. International Journal of Solids and Structures 2006; 43(10): 3197–3212.

[8] Sweeting R.D., Thomson R.S.: The effect of thermal mismatch on Z-pinned laminated composite structures. Composite Structures 2004; 66(1-4): 189-195.

[9] Mouritz A.P., Chang P.: Tension fatigue of fibre-dominated and matrix-dominated laminates reinforced with z-pins. International Journal of Fatigue 2010; 32(4): 650-658..

[10] Zhang A., Liu H.Y., Mouritz A., Mai Y.W.: Experimental Study and Computer Simulation of Z-Pin Reinforcement under Cyclic Fatigue. Composites Part A 2008; 39(2): 1501-1513.

[11] Partridge IK, Cartié D.D.R.: Delamination resistant laminates by Z-Fiber pinning: Part I manufacture and fracture performance. Composites Part A 2005; 36(1): 55–64.

[12] Partridge IK, Cartié D.D.R., Troulis M.: Delamination of Z-pinned carbon fibre reinforced laminates. Composites Science and Technology 2006; 66(6): 855-861.

[13] Dai S.C., Yan W., Liu H.Y., Mai Y.W.: Experimental study of z-pin bridging law by pullout test. Composites Science and Technology 2004; 64(16): 2451-2457.

[14] Cartié D.D.R., Cox B.N., Flech N.A.: Mechanisms of crack bridging by composite and metallic rods. Composites Part A 2004; 35(11): 1325-1336.

[15] Gornet L., Ijaz H., Cartié D.D.R.: Inelastic Interface Damage Modeling with Friction Effects: Application to Z-Pinning Reinforcement in Carbon Fibre Epoxy Matrix Laminates. Journal of Composite Materials 2010; 44(17): 2067-2081.

[16] Lefèbure P.: “Assembly of dry Carbon Preforms by a Z-pinning technology”, SAMPE Europe Technical Conference, SETEC January 2006.

[17] Greenhalgh E., Lewis A., Bowen R., Grassi M.: Evaluation of toughening concepts at structural features in CFRP – Part I: Stiffener pull-off. Composites Part A 2006; 37(10): 1521-32.

[18] Javier Toral Vasquez.: Identification et modélisation du comportement des structures composites assemblées par cloutage. PHd Thesis Université de Toulouse. http://oatao.univ-toulouse.fr/4181/ (in French).

[19] Jiang W.G., Yao M.S., Walton J.M.: A concise finite element model for simple straight wire rope strand. International Journal of Mechanical Sciences 1999; 41(2): 143-161.

[20] Zhang X, Liu HY, Mai YW, Diao XX.: On steady-state fibre pull-out I The stress field. Composites Science and Technology 1999; 59: 2179-2189.

[21] Fu SY, Yue CY, HU X, Mai YW.: Analyses of the micromechanics of stress transfer in single and multi-fiber pull-out test. Composites Science and Technology 2000; 60: 569-579.

[22] Samcef User's Guide, by Samtech Group, Liege, Belgium. www.Samtech.com.

FIGURES

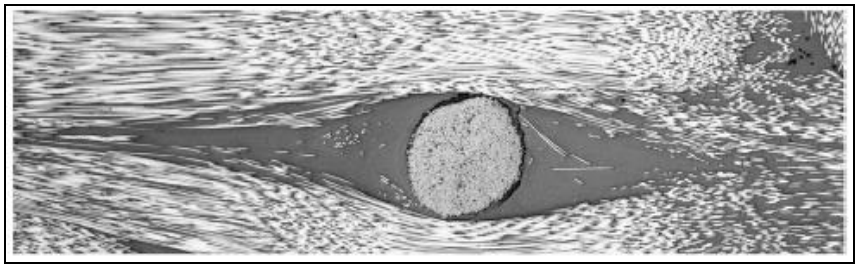

Figure 1: Resin pocket around a pin (reproduced from [7]).

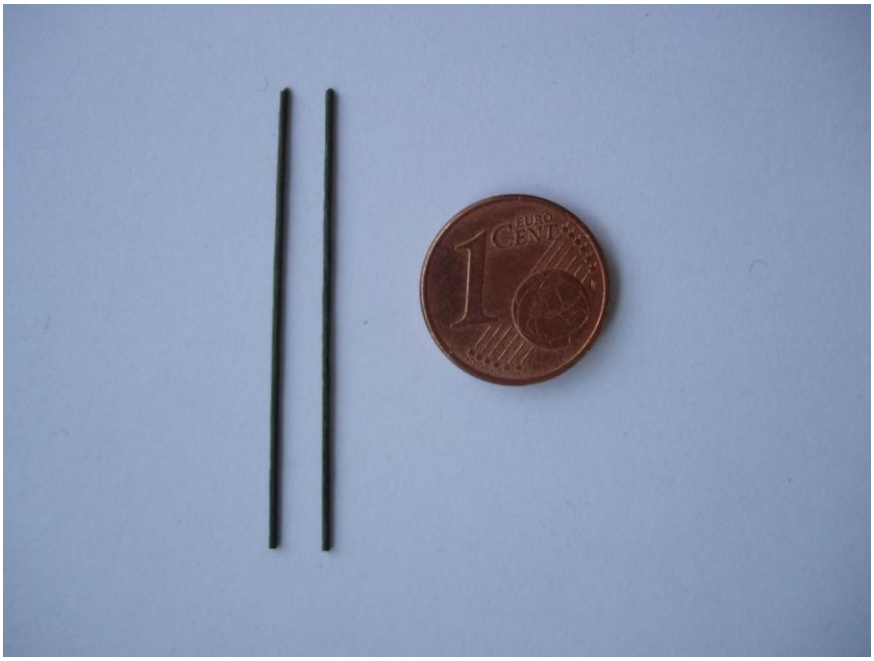

(a)

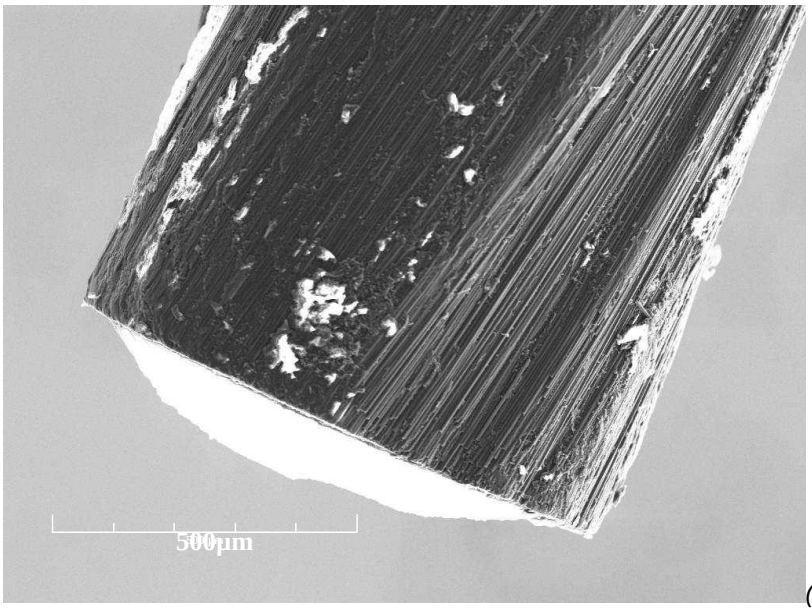

(b)

Figure 2: (a) Hexcel's pins, (b) twisted shape (0.7 mm).

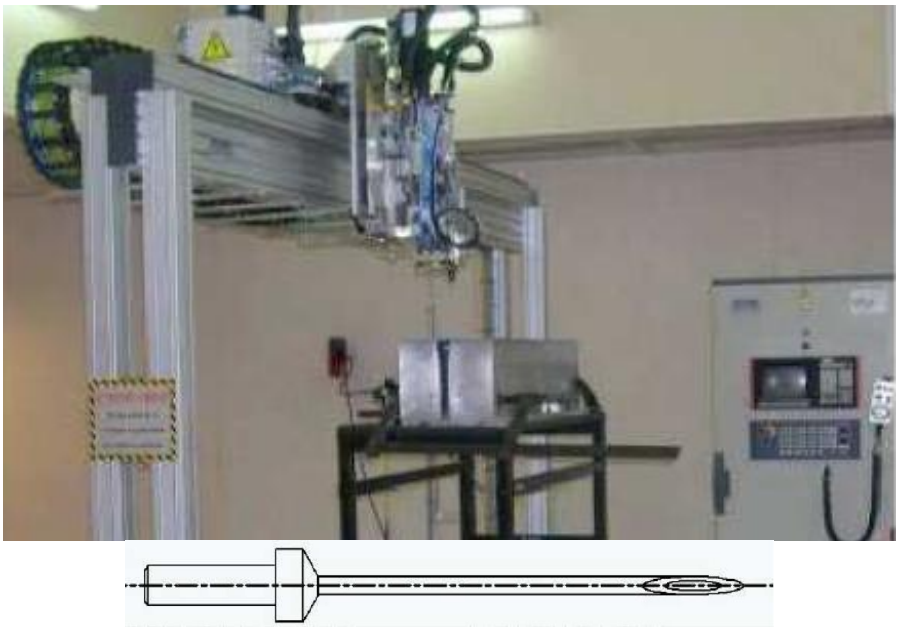

Figure 3: The EADS-IW Z-Pinning machine and vibrating needle.

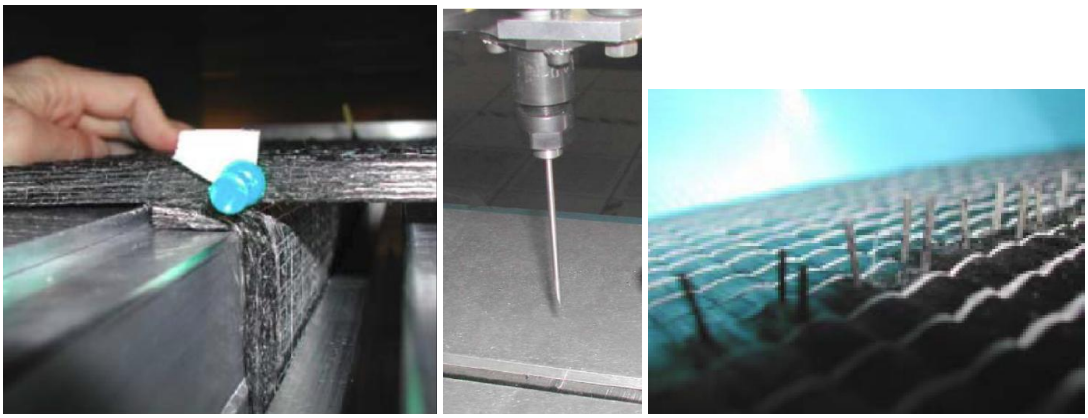

Figure 4: Insertion process.

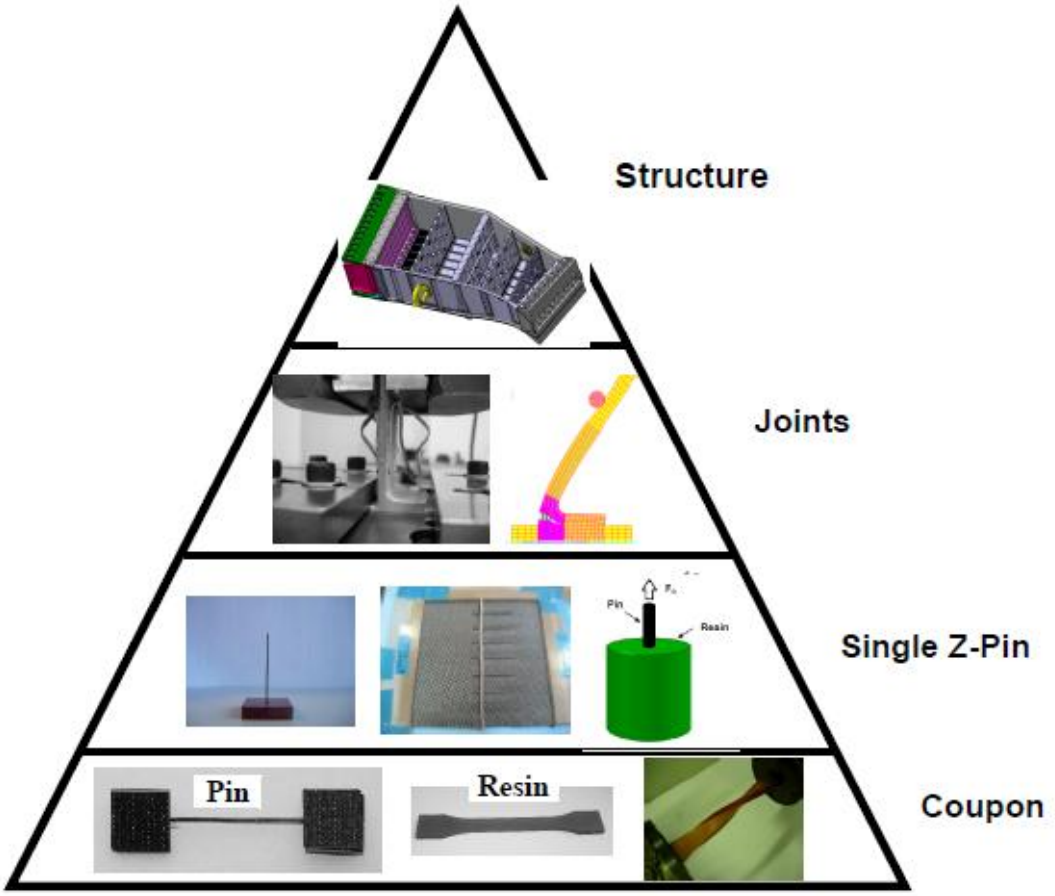

Figure 5: Multi-level analysis.

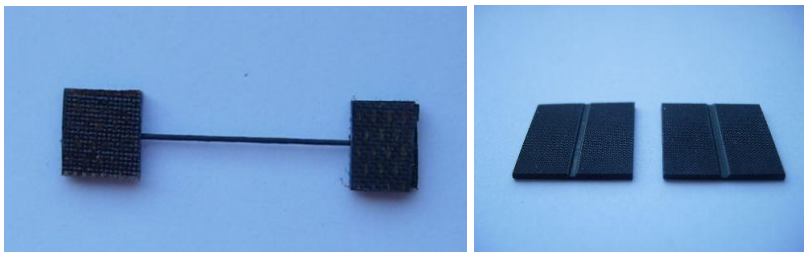

Figure 6: Single pin specimen with loading plates.

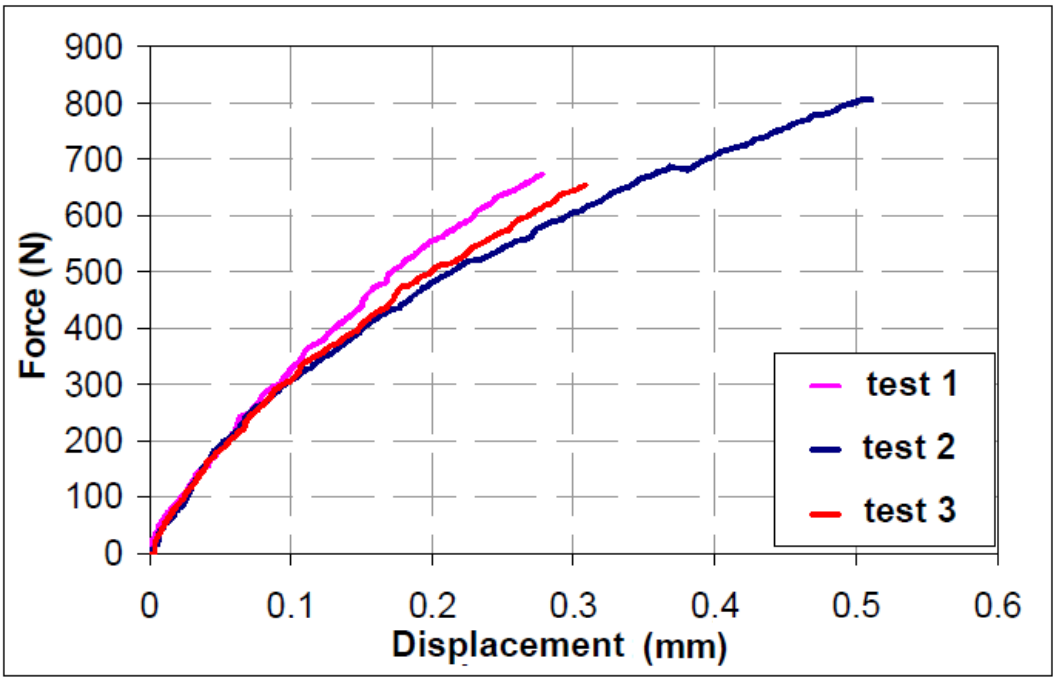

Figure 7: Typical load-displacement curves for Z- pins 0.7 mm diameter under tension.

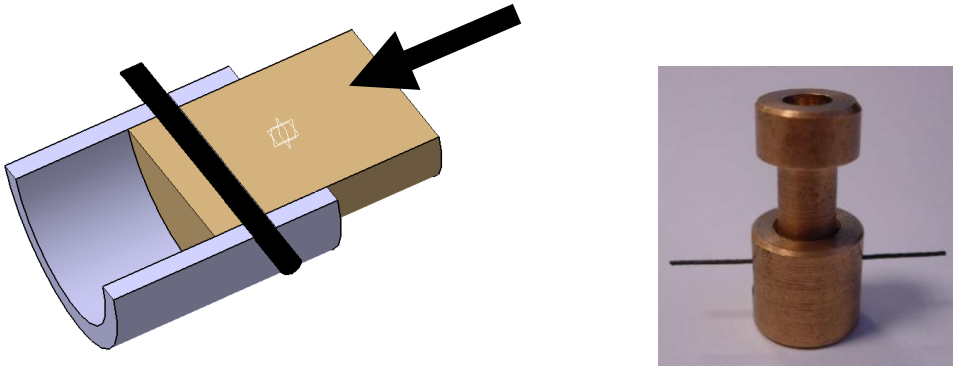

Figure 8: Shear device for single Z-pins.

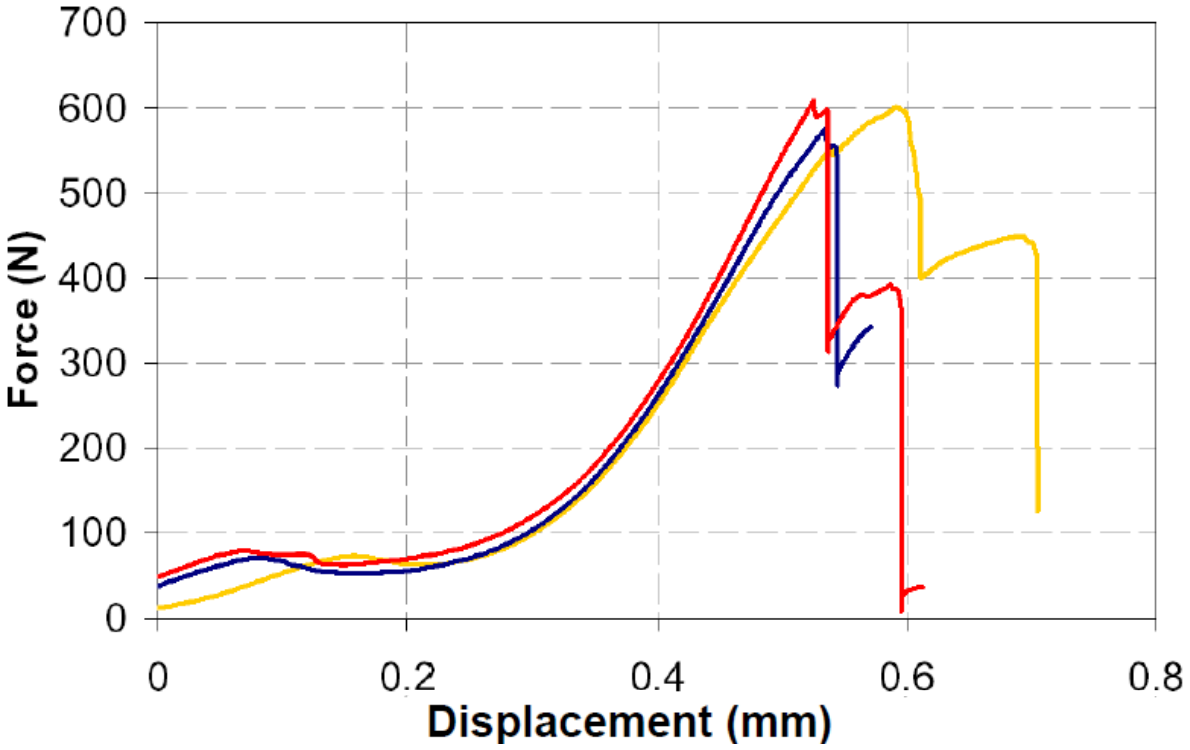

Figure 9: Shear tests force/displacement curves for 0.7 mm pins.

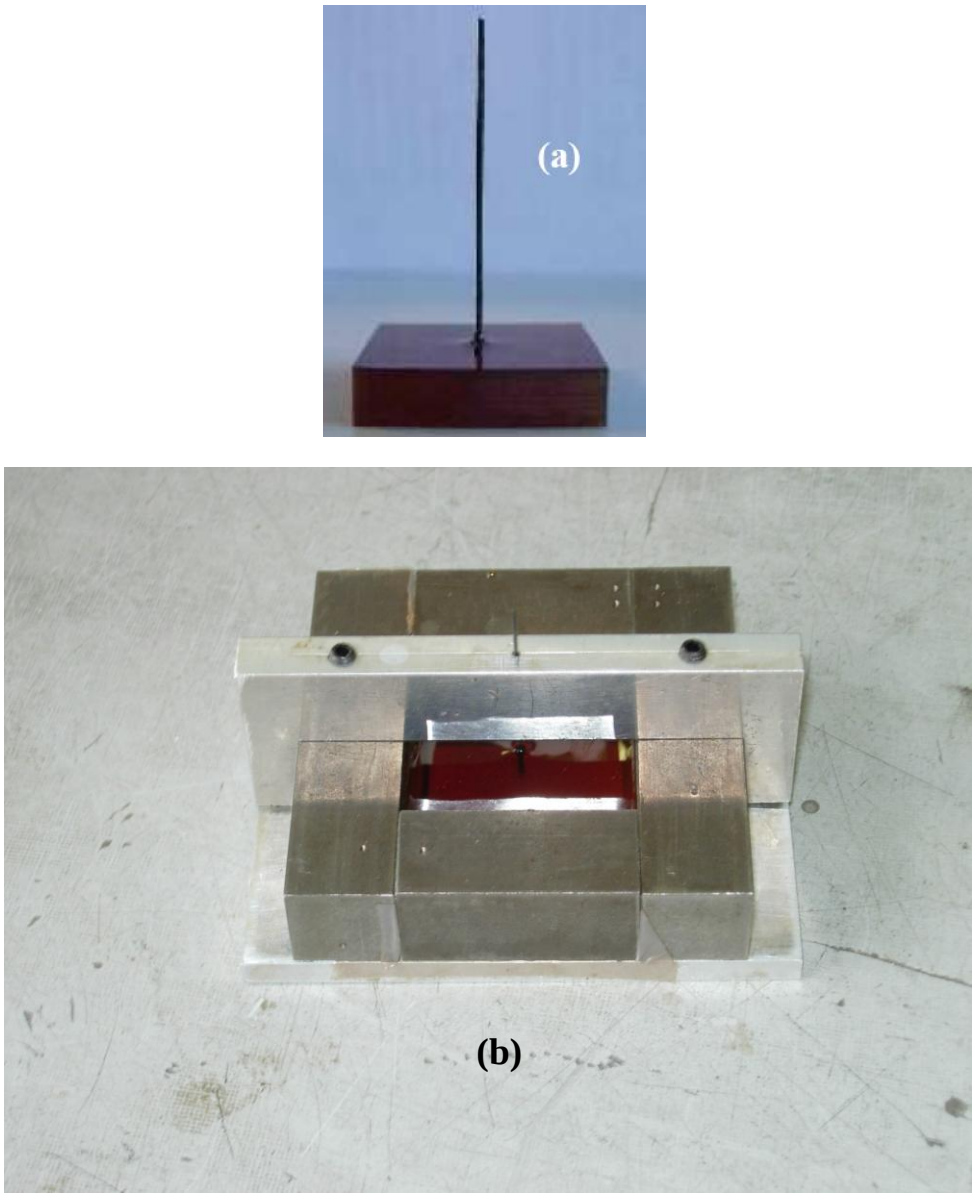

Figure 10: Specimen for pull-out test a single pin in net resin (a) and its mould (b).

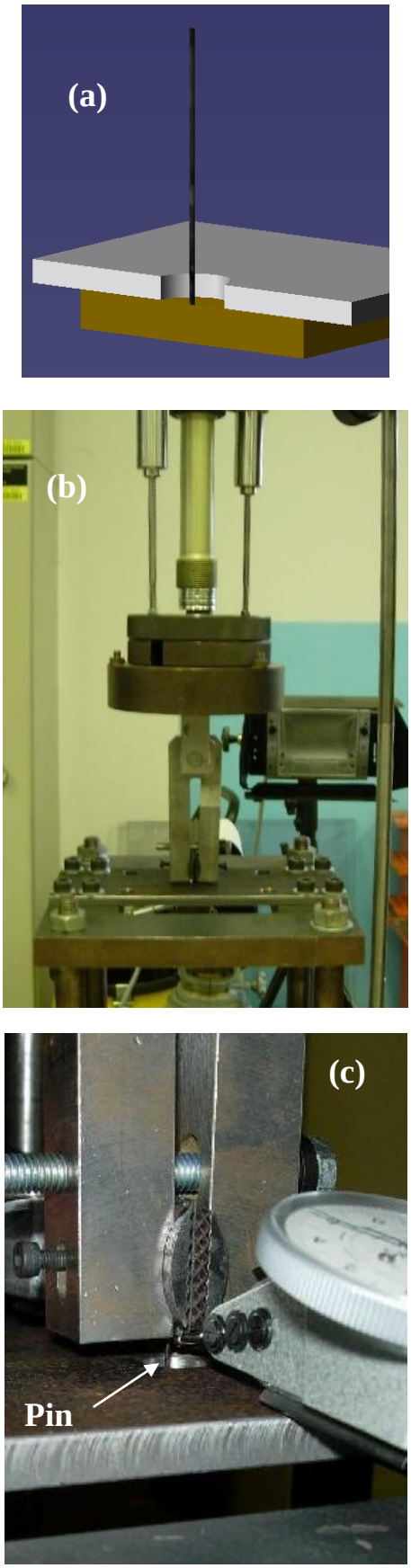

Figure 11: Pull-out test of a single pin in net resin: (a) principle, (b) test device, (c) zoom on the grips.

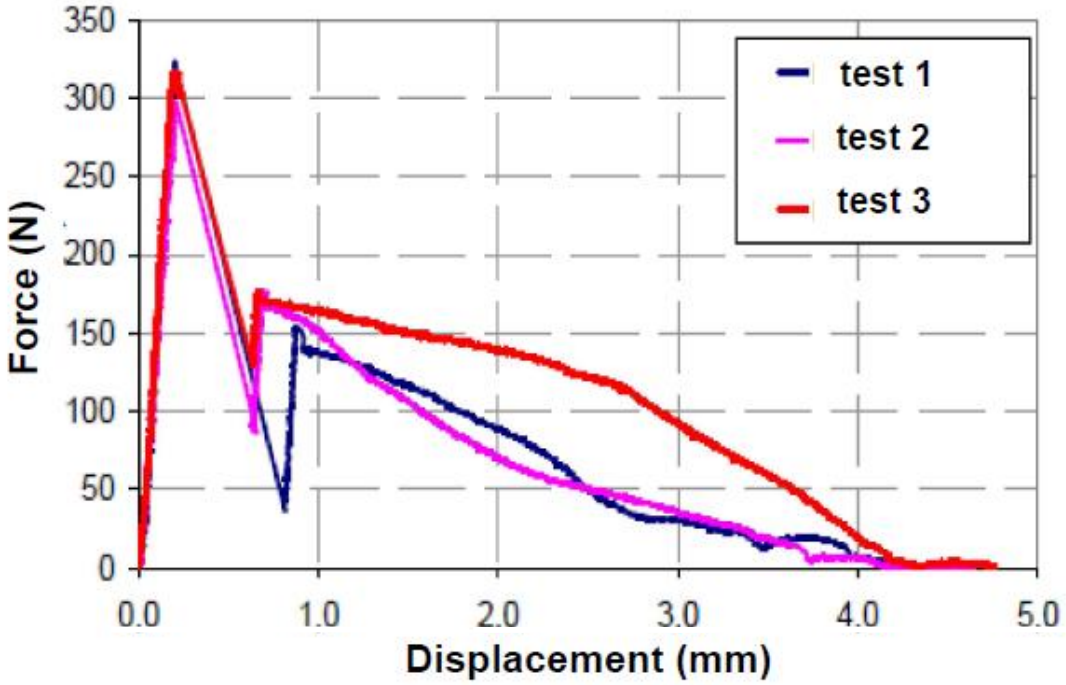

Figure 12: Typical pull-out force/displacement curves.

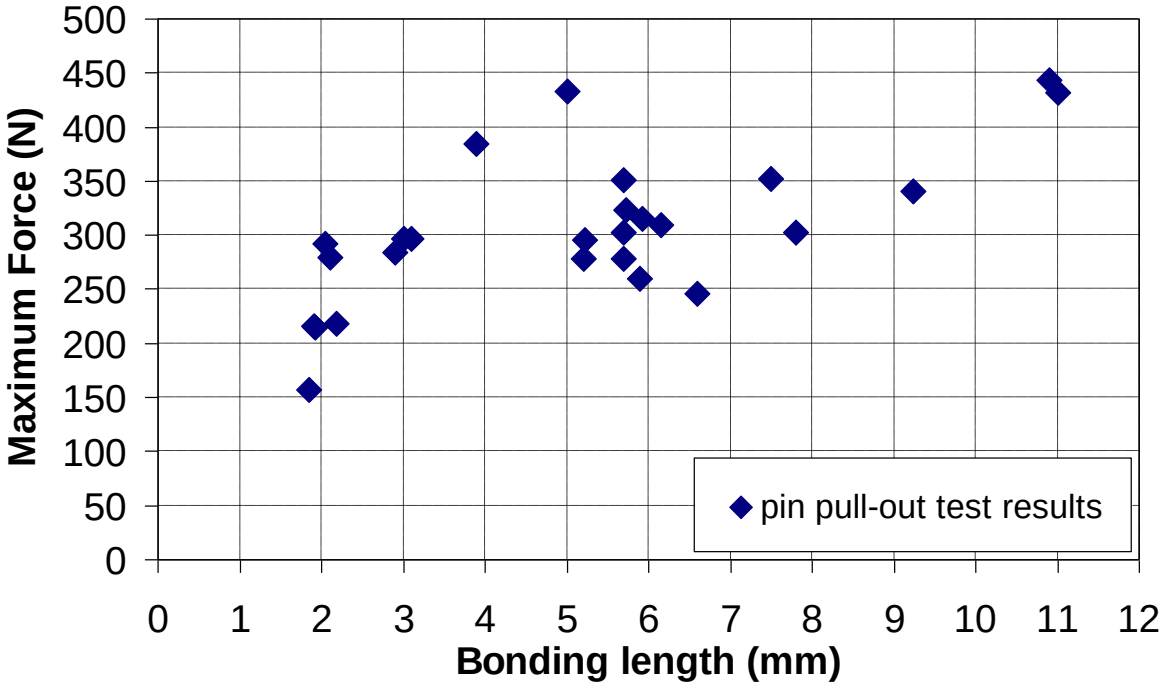

Figure 13: Experimental pin pull-out strength values.

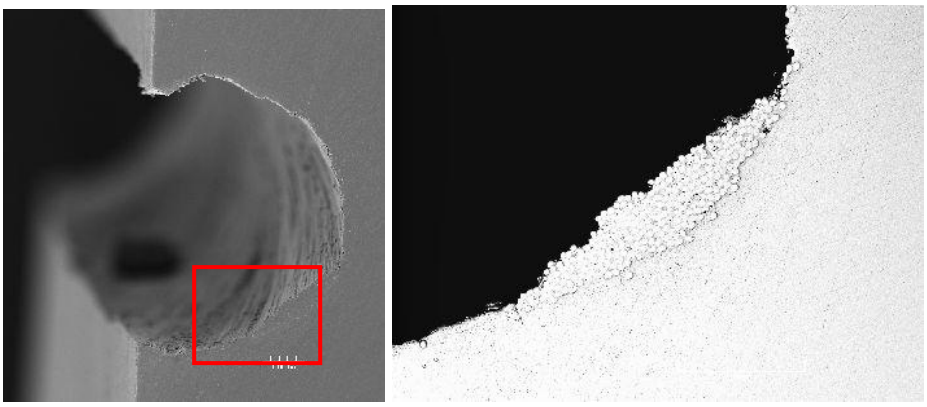

Figure 14: Detail of a strand of fibres which remained bonded to the resin.

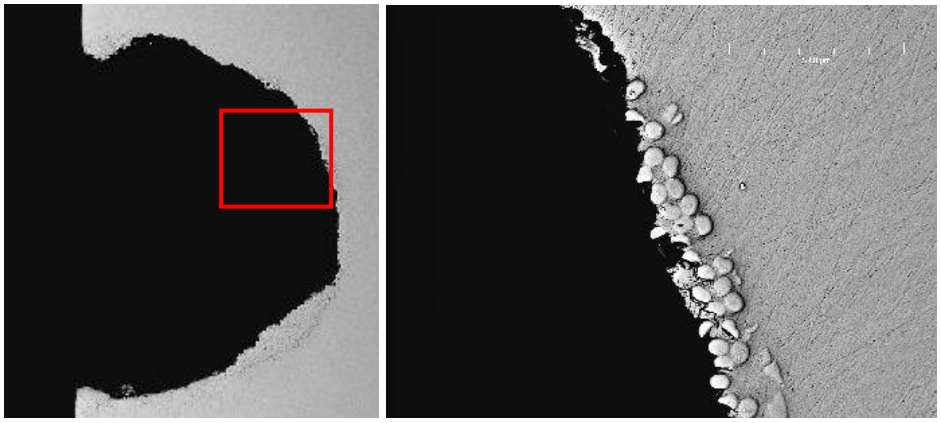

Figure 15: Detail of isolated fibres which remained bonded to the resin.

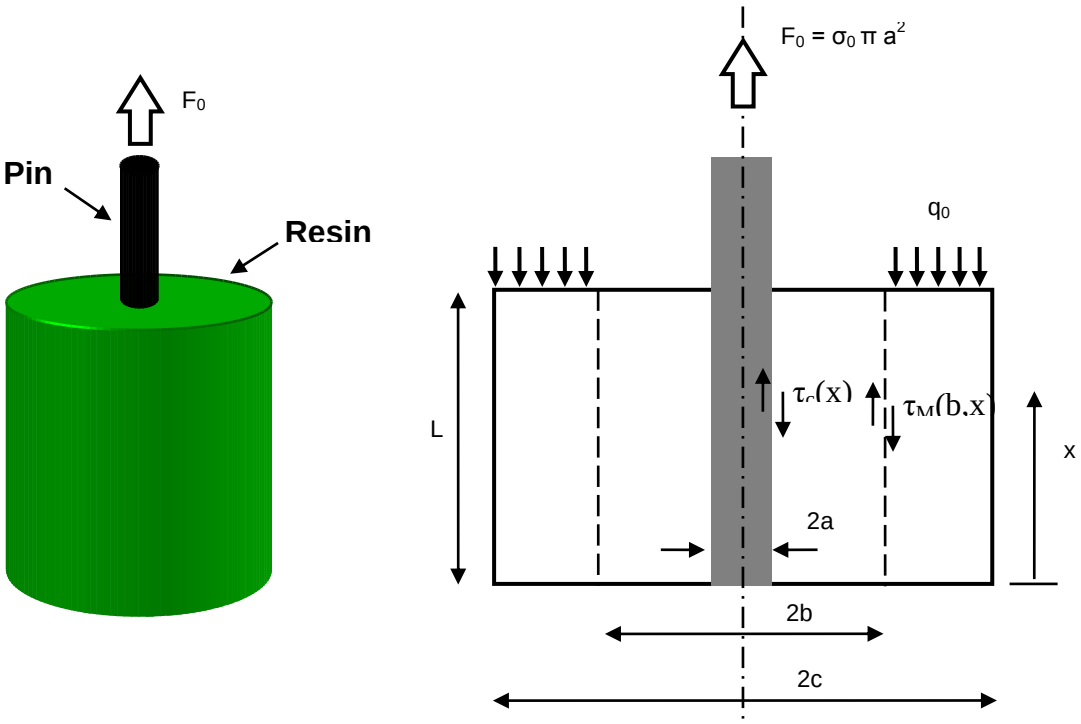

Figure 16: Modelling Z-pin pull-out.

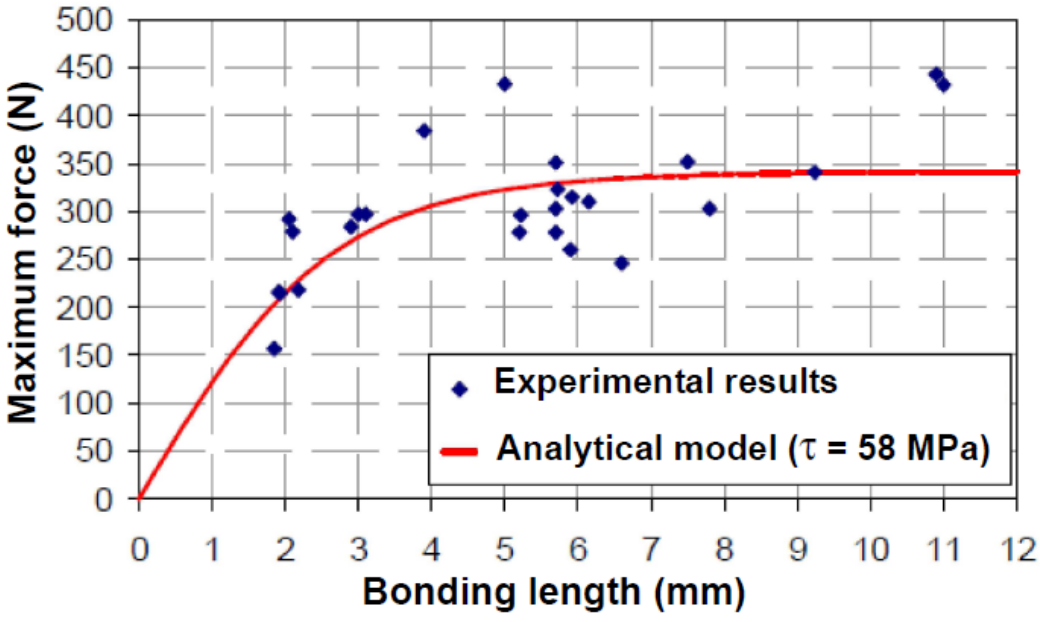

Figure 17: Experimental pin pull-out strength values compared to analytical model results.

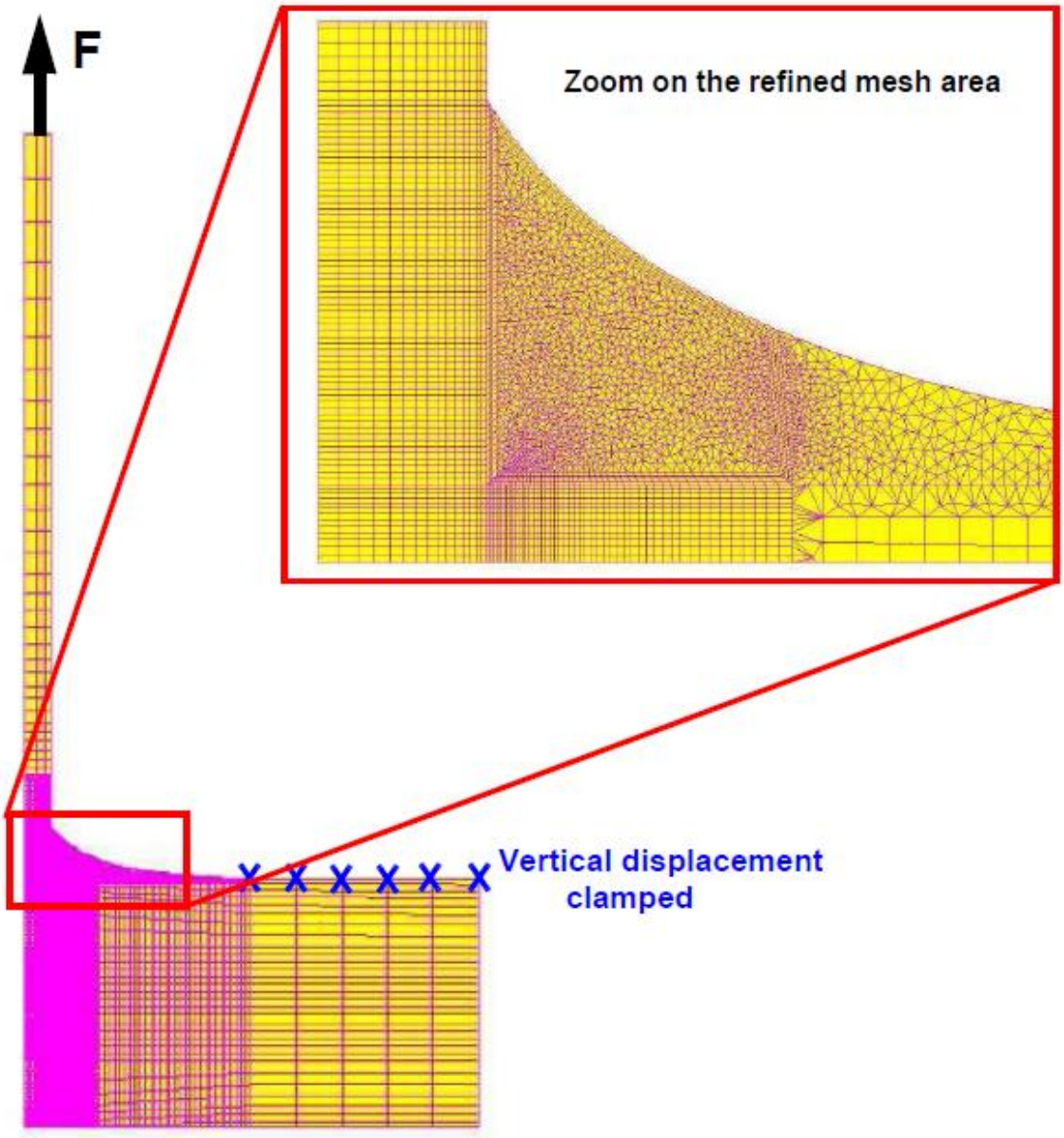

Figure 18: Detailed Finite Element model

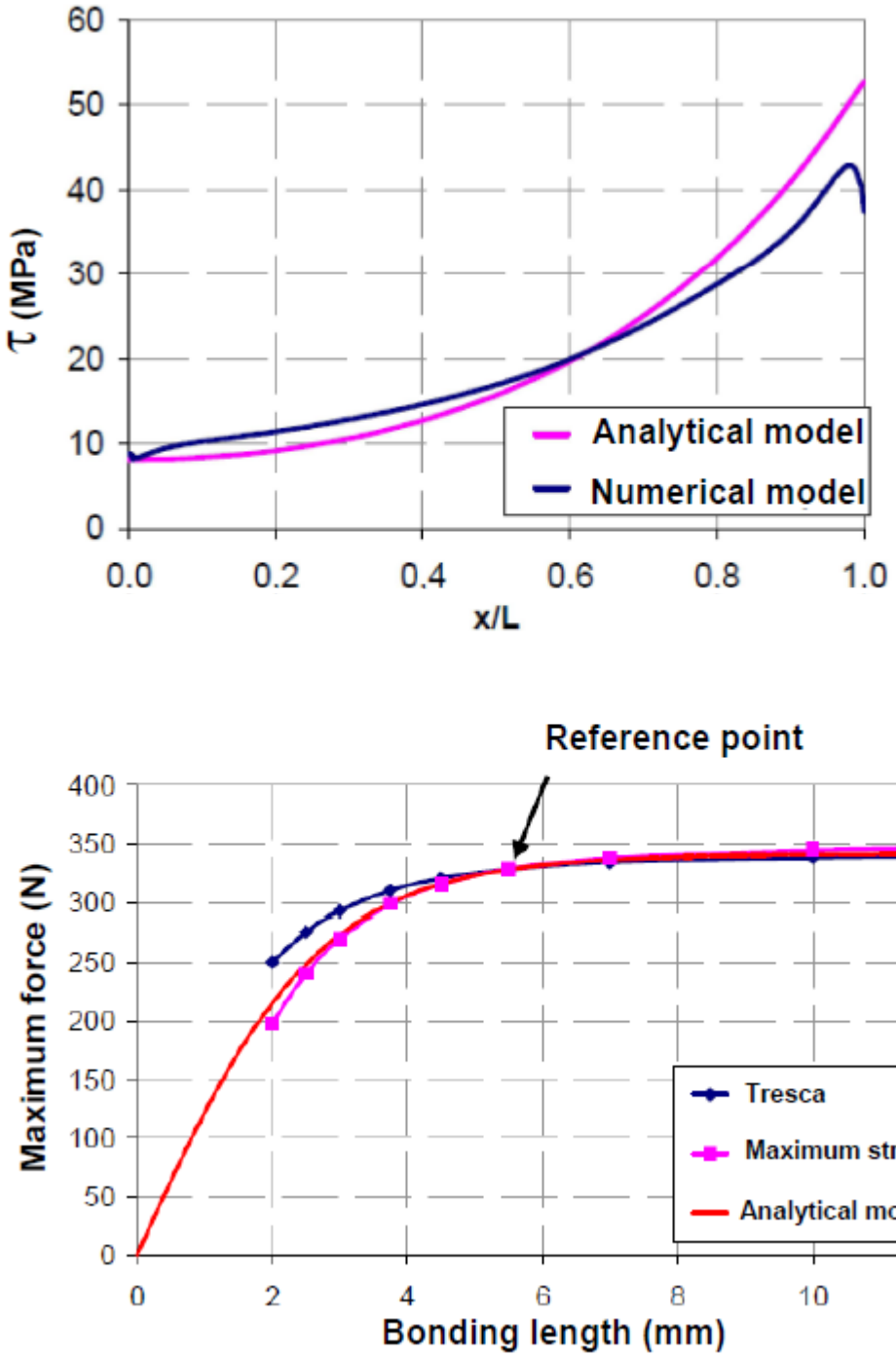

Figure 19: Comparison of shear stress and debonding load found by FEA with analytical results.

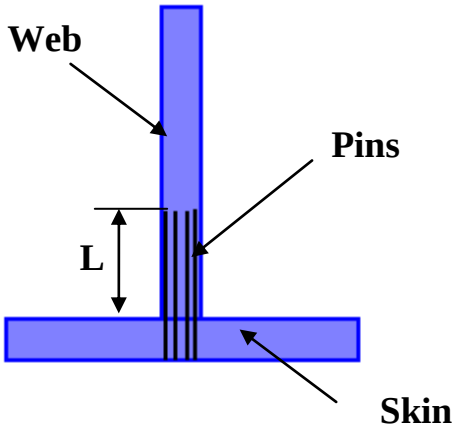

Figure 20: Typical T-Joint.

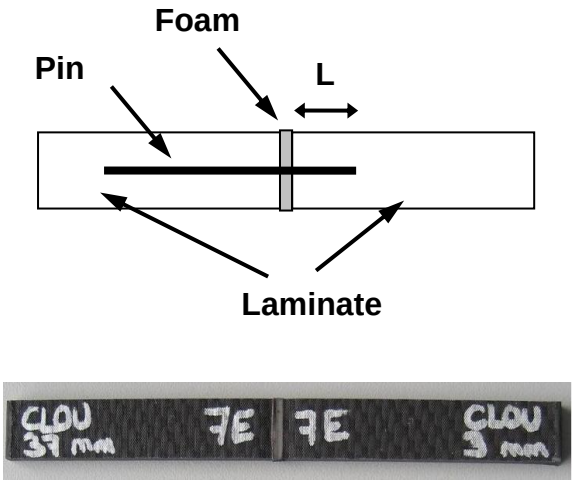

Figure 21: Pin inside laminate: Pull-out specimen diagram principle.

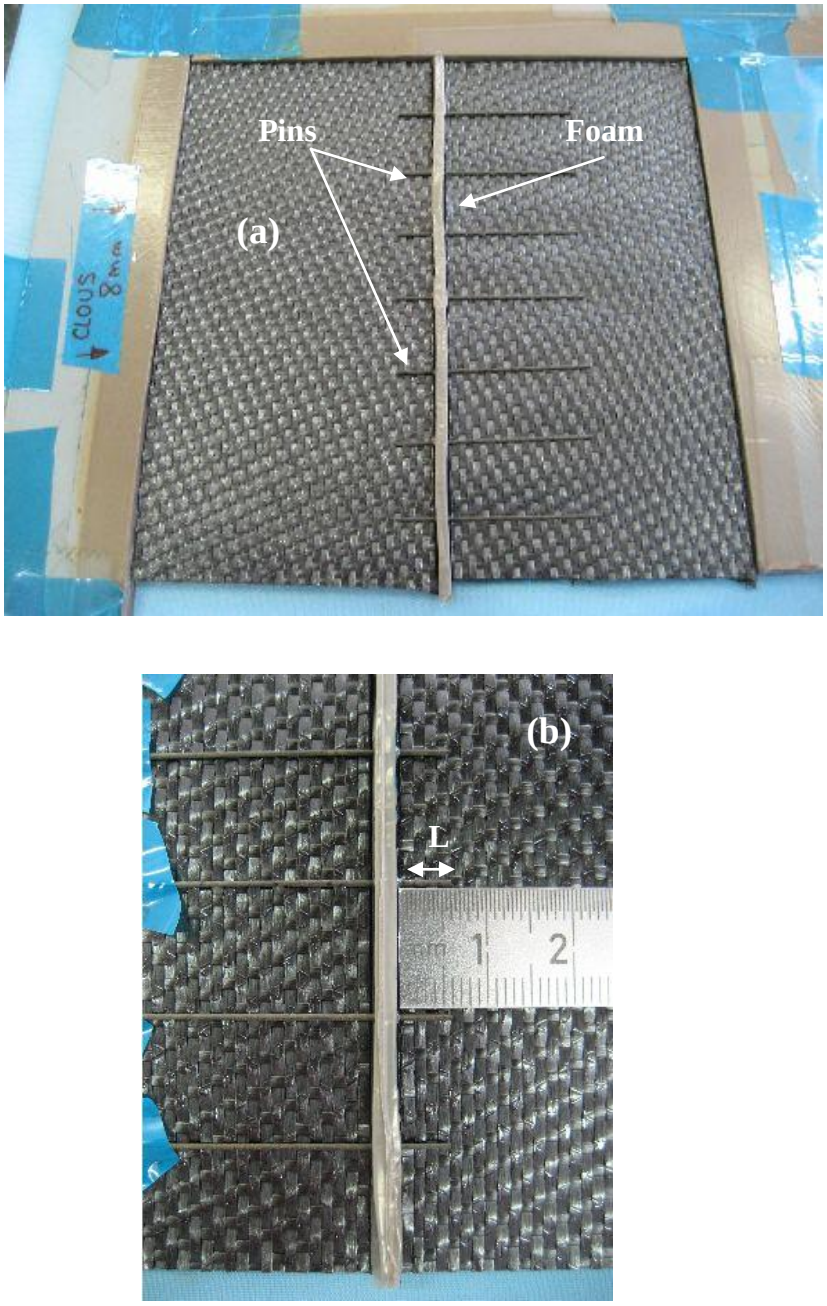

Figure 22: Manufacturing process details of the plate with Z-pins: (a) insertion of Z-pins at the middle of thickness when laying up, (b) checking of the insertion depth.

Figure 23: Pin pull-out from laminate test assembly

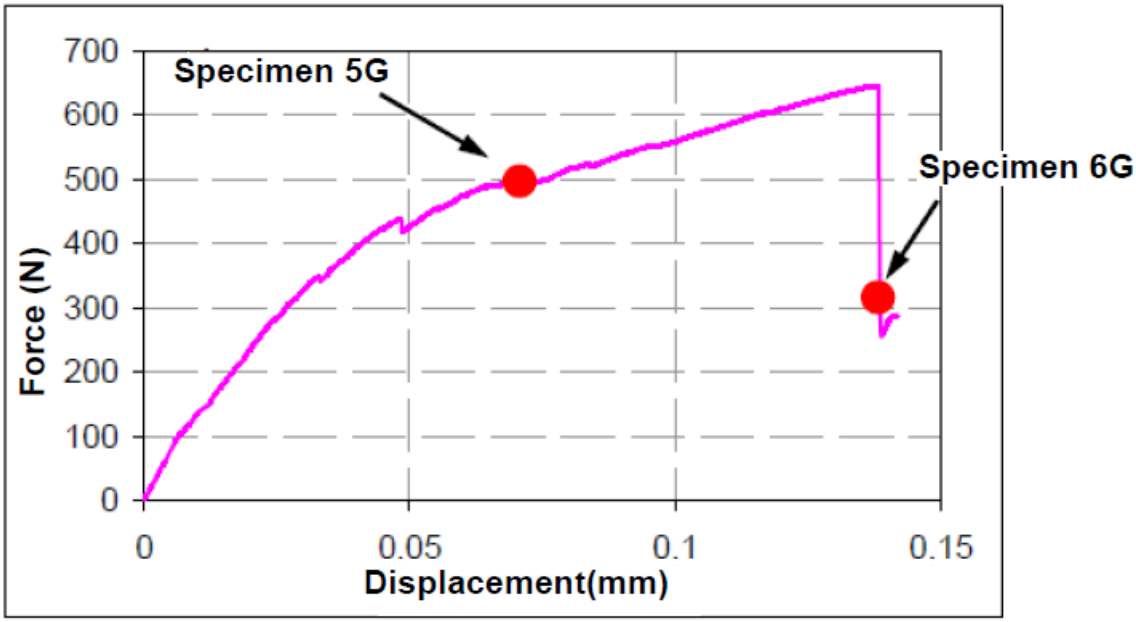

Figure 24: Typical load/displacement curve of pin pull-out from laminate

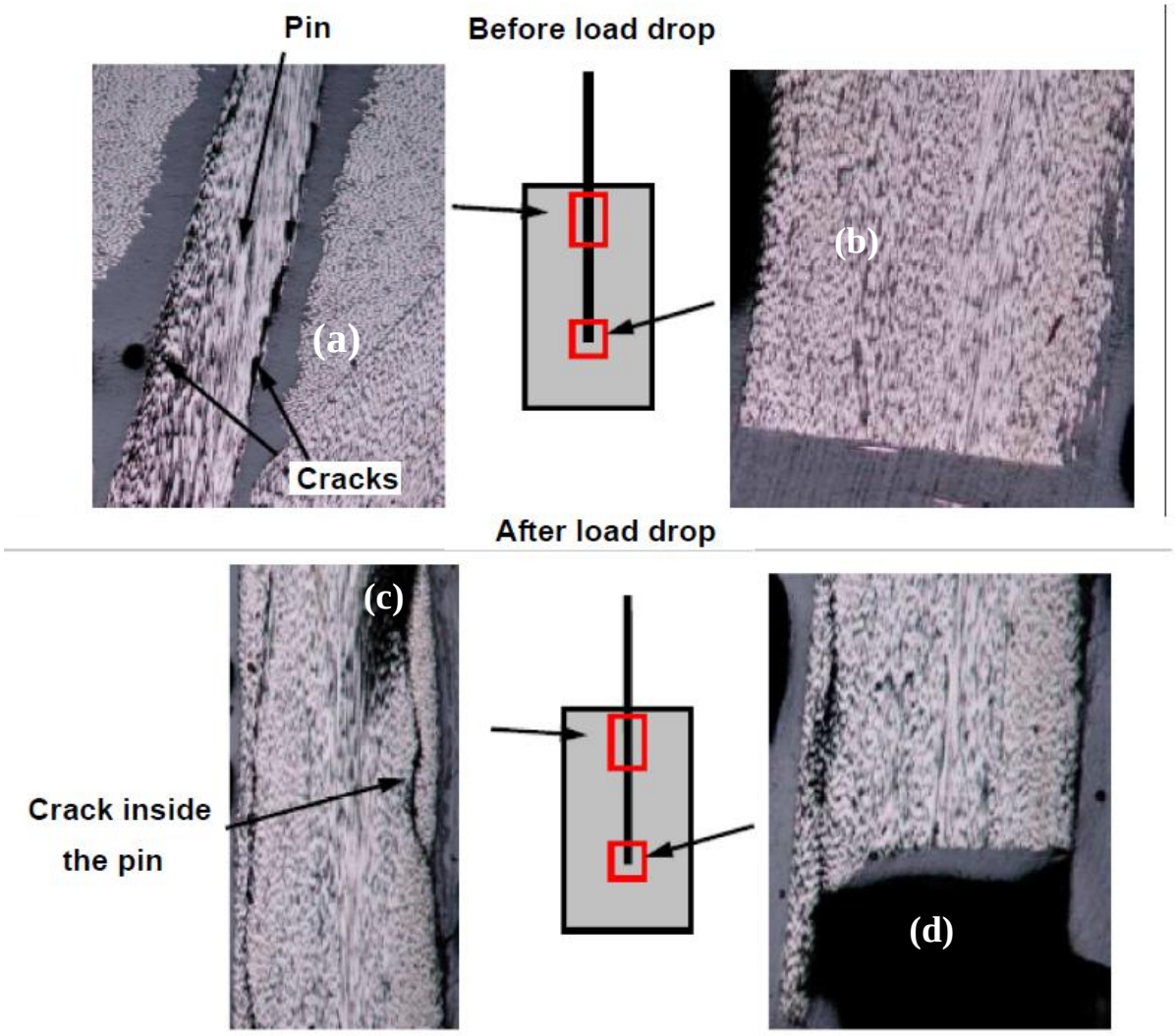

Figure 25: Micrographic analysis before (top) and after (bottom) load drop

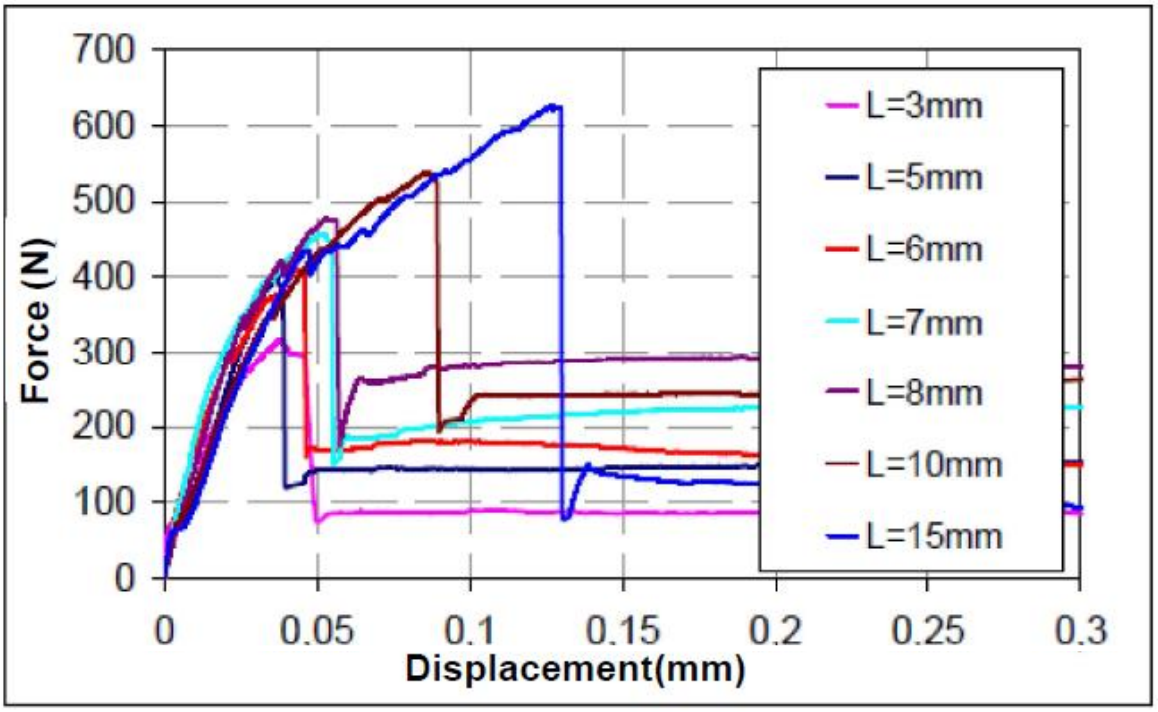

Figure 26: Insertion depth (L) influence on pin pull-out behavior

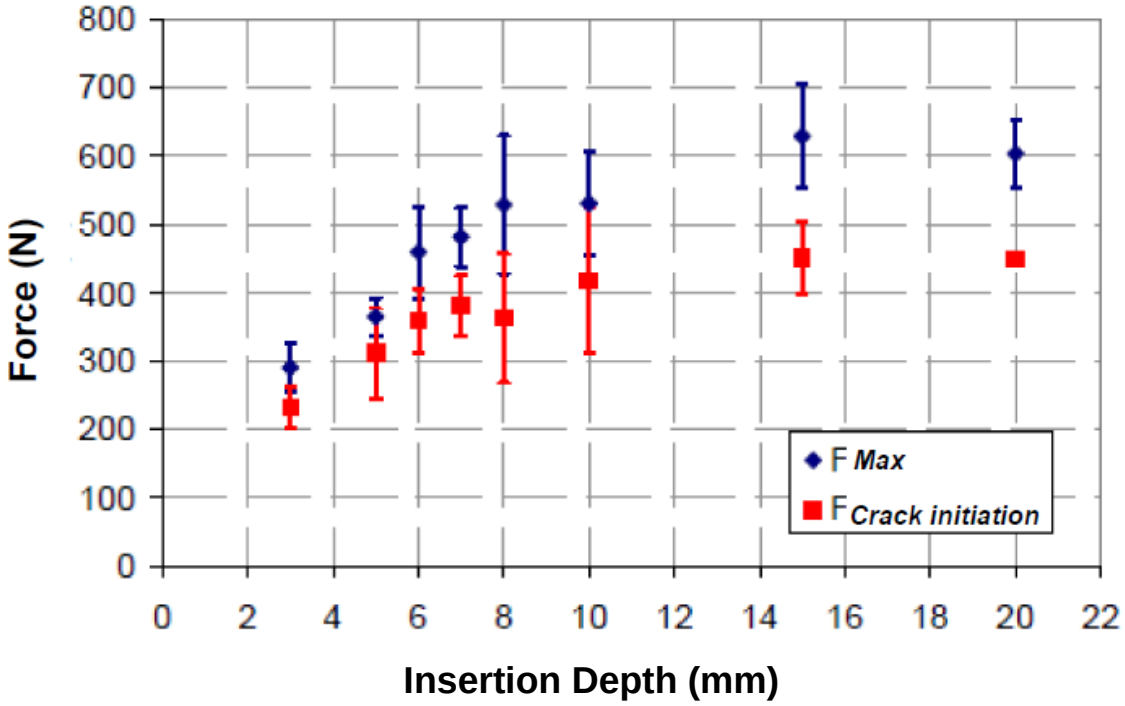

Figure 27: Crack initiation load (red) and maximum applied load (blue). Pin pull-out from laminate

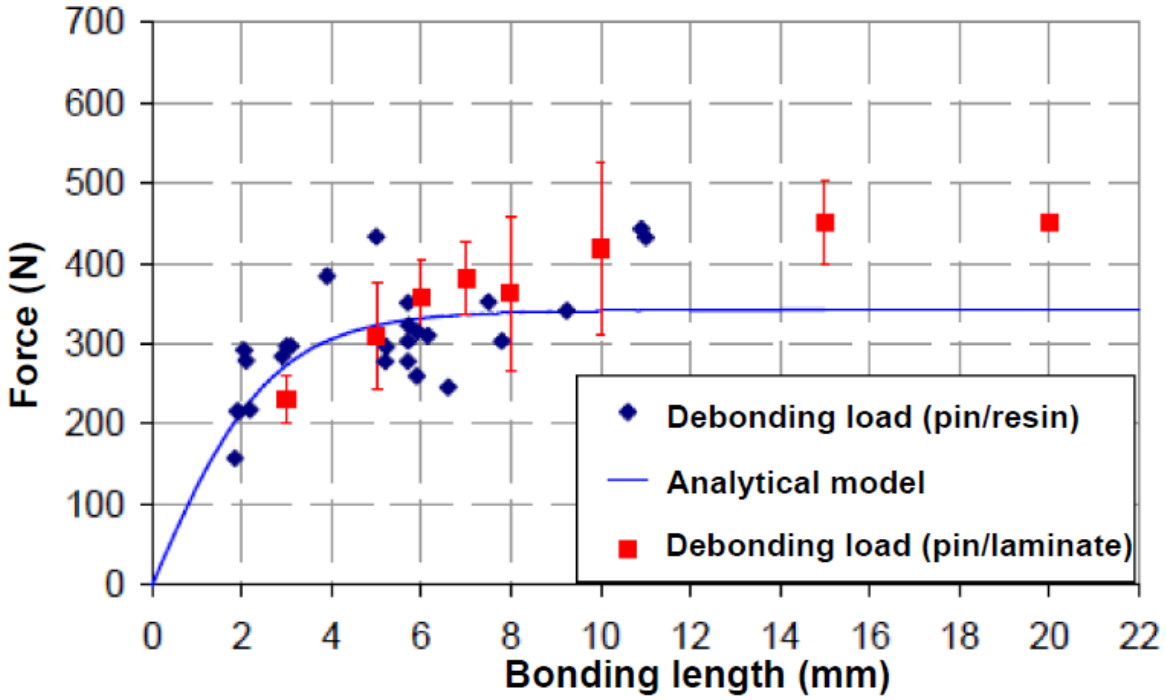

Figure 28: Crack initiation load from pin pull-out from laminate test results compared to pin debonding load from net resin and analytical debonding model results.

TABLES

Diameter (mm)	Maximum applied load (N)		Linear increase slope (N/mm)	
	Mean value	Standard deviation	Mean value	Standard deviation
0.7	288	16.8	1396	228

Table 1: Shear test results

Insertion depth (mm)	Number of Specimens	Reference	Displacement measurement
3	7	E	LVDT
5	4	D	LVDT
6	4	H	LVDT
7	3	H	LVDT
8	7	F	LVDT
10	4	D	LVDT
15	3	G	LVDT
15	3	I	LVDT + Cameras
20	4	A	LVDT

Table 2: Pin inserted in laminate specimens